HHS Public Access

Author manuscript

Proc SPIE Int Soc Opt Eng. Author manuscript; available in PMC 2017 June 12.

Published in final edited form as:

Proc SPIE Int Soc Opt Eng. 2017 February 11; 10132: . doi:10.1117/12.2254064.

Monte Carlo investigation of backscatter point spread function for X-ray imaging examinations

Zhenyu Xiong[a,c], **Sarath Vijayan**[a,c], **Stephen Rudin**[a,b,c], and **Daniel R. Bednarek**[a,b,c]

[a]University at Buffalo, Department of Physiology and Biophysics, 124 Sherman Hall, 3435 Main Street, Buffalo, New York 14214, United States

[b]University at Buffalo, Department of Radiology, 319A Sherman Hall, 3435 Main Street, Buffalo, New York 14214, United States

[c]Toshiba Stroke & Vascular Research Center, 875 Ellicott Street, Buffalo, New York 14203, United States

Abstract

X-ray imaging examinations, especially complex interventions, may result in relatively high doses to the patient's skin inducing skin injuries. A method was developed to determine the skin-dose distribution for non-uniform x-ray beams by convolving the backscatter point-spread-function (PSF) with the primary-dose distribution to generate the backscatter distribution that, when added to the primary dose, gives the total-dose distribution. This technique was incorporated in the dose-tracking system (DTS), which provides a real-time color-coded 3D-mapping of skin dose during fluoroscopic procedures. The aim of this work is to investigate the variation of the backscatter PSF with different parameters. A backscatter PSF of a 1-mm x-ray beam was generated by EGSnrc Monte-Carlo code for different x-ray beam energies, different soft-tissue thickness above bone, different bone thickness and different entrance-beam angles, as well as for different locations on the SK-150 anthropomorphic head phantom. The results show a reduction of the peak scatter to primary dose ratio of 48% when X-ray beam voltage is increased from 40 keV to 120 keV. The backscatter dose was reduced when bone was beneath the soft tissue layer and this reduction increased with thinner soft tissue and thicker bone layers. The backscatter factor increased about 21% as the angle of incidence of the beam with the entrance surface decreased from 90° (perpendicular) to 30°. The backscatter PSF differed for different locations on the SK-150 phantom by up to 15%. The results of this study can be used to improve the accuracy of dose calculation when using PSF convolution in the DTS.

Keywords

Diagnostic x-ray dosimetry; backscatter; point spread function; Monte Carlo simulation

1. INTRODUCTION

Fluoroscopically-guided interventional (FGI) procedures may result in patient skin doses exceeding the threshold for radiation induced skin injuries. Many of these interventions can be prolonged and result in a significant exposure to the patient's skin.[1] The biological damage to the tissue is associated with threshold dose levels for various deterministic

effects. It is thus important to determine the patient's skin dose as accurately as possible. A substantial component of dose to the skin is due to backscattered radiation from the patient. Typically, backscatter has been shown to increase the skin dose for large fields by about 30% to 60% over the primary at the center of the x-ray field.[2] Backscatter factors (BSF) have been measured and calculated by a number of investigators; their results have shown the backscatter factor to be dependent on the size of the field, the thickness of the patient and the beam energy.[3–4]

These backscatter factors can be used to convert the incident air kerma to the entrance surface dose at the center of a uniform beam of a given field size. However, the backscatter contribution to the skin dose will not be uniform across the field from the center to the edge, but will decrease toward the periphery of the field and extend beyond the field boundary. Furthermore, when the primary beam is not uniform, a single backscatter factor will not be able to describe the distribution of backscatter dose. For example, beam shaping devices like region-of-interest (ROI) attenuators[5–8] and compensation filters[9] modify the primary beam distribution and concomitantly the backscatter distribution.

We have previously developed a dose tracking system (DTS) [10–20] to provide a real-time color-coded 3D-mapping of skin dose. To improve the accuracy of dose calculation, we proposed a method for the estimation and automatic mapping of cumulative skin dose for spatially-shaped X-ray fields through the convolution of a backscatter "point spread function" (PSF) with the primary dose distribution.[21,22] To improve the accuracy of our backscatter PSF convolution method, this study investigated the variation of backscatter PSF with variation of a number of parameters such as beam energy, incident angle, and object properties.

2. METHOD AND MATERIALS

2.1 Monte Carlo Simulation of backscatter PSF

To determine the spatial distribution of backscatter to the patient's skin, a backscatter PSF normalized to the primary exposure was determined for both a uniform water phantom and an anthropomorphic head phantom by simulating a pencil beam with EGSnrc Monte Carlo software.

To generate the spectra used for the backscatter PSF determination, the x-ray tube of the Toshiba Infinix C-Arm System was modeled by BEAMnrc/EGSnrc. The photon fluence was determined from the phase space file calculated by the BEAMnrc. The BEAMDP was used to calculate the spectra based on the photon fluence.

The dose profile for a 1 mm square primary x-ray beam was obtained without and with the phantom, consequently determining the primary and the total (primary + scatter) dose distributions, respectively. The primary dose distribution is subtracted from the total dose for estimating the scatter variation and this is subsequently normalized to the primary intensity to obtain the scatter-to-primary point spread function.

The surface dose distributions were calculated using the DOSxyznrc/EGSnrc. The voxel size used in the simulation was 1×1×1 mm^3. We used a source type 1 (parallel rectangular beam incident from any direction) to simulate the 1×1 mm^2 pencil beam projected on the phantom. We turned on the following low energy physics options for accurate simulation: electron impact ionization, bound Compton scattering, photoelectron angular sampling, atomic relaxation, Rayleigh scattering and simple bremsstrahlung angular sampling. The NIST data were used for all bremsstrahlung cross section simulations and XCOM was used for photo-absorption and Rayleigh-scattering total cross sections. We implemented the EXACT boundary crossing algorithm which utilizes a single scattering mode to cross boundaries. Each calculation used 5×10^9 incident particles. The polychromatic beam simulations in the following used an 80kVp beam with a 3.1 mm Al half-value layer (HVL) which modeled the spectra from the Infinix C-Arm system with 1.8 mm Al added filtration.

2.2 Parameter variation

Backscatter PSF vs keV—A homogeneous water phantom (20×20×20 cm^3) was irradiated by mono-energetic photon pencil beams perpendicular to the phantom surface over a range of keV's (30 keV-120 keV). We compared the absolute backscatter dose distribution and the scatter/primary ratio. To show the comparison of the PSF more clearly, we convolved the PSF at different keVs and for different field sizes (5 cm, 10 cm and 20 cm) to derive the backscatter factors at the center of the field.

Backscatter PSF vs thickness of soft tissue above bone—The thickness of skin and soft tissue on the entrance surface above bone in different locations of the body is different. To investigate the change in backscatter PSF for different soft tissue thickness's above the bone, an inhomogeneous phantom containing a thin water layer (1, 3, 5 and 20 mm) over a 0.6 cm thick bone (which is the average thickness of the human cranium) was used as shown in Figure 1. The phantom (20×20×20 cm^3) was irradiated by an 80 kVp photon pencil beam perpendicular to the phantom surface,. The density of bone equal to 1.85 g/cm3, and the PEGS4 cross-section data of bone (ICRPBONE521ICRU) was used. The bone was over about 20 cm water to provide sufficient backscattering. To show the effect of the differences in PSF more clearly, we calculated the BSF for different water thickness on the entrance surface above the bone layer by convolution of the PSF simulated by EGSnrc for a 20 cm square field size.

Backscatter PSF vs thickness of bone under soft tissue layer—The thickness of the bone varies from individual to individual and with location on different parts of the body. To investigate the change in backscatter PSF for different bone thickness, an inhomogeneous phantom containing a 5 mm thin water layer over a bone layer of different thicknesses (2.5, 7.5 and 12.5 mm) was used as shown in Figure 1. The phantom (20×20×20 cm^3) was irradiated by an 80 kVp pencil beam perpendicular to the phantom surface.

Backscatter PSF vs incident angle—The x-ray beam is not always perpendicular to the patient surface because some locations of patient surface are curved and the x-ray beam itself is divergent or may extend to the side of the patient. To investigate the change in backscatter PSF for different entrance beam angles, a homogeneous water phantom

($20\times20\times20$ cm^3) was irradiated by an 80 kVp pencil beam which was incident at 90° (perpendicular), 60° and 30° to the phantom surface as shown in Figure 2.

Backscatter PSF for head phantom—We also compared the backscatter PSF on several locations of an SK-150 anthropomorphic head phantom (Phantom Laboratory, Salem, NY). The phantom was similar in dimensions and materials density with a real head and contained a human skull. We did a CT scan of the head phantom and used the DICOM file of it to construct an .egsphant file to describe the SK-150 head phantom by using a Visual C++ program. This file includes the coordinate, material and density information for EGSnrc simulation.

3. RESULTS

Figure 3 shows the backscatter PSF of a 1 mm pencil beam for the 20 cm thick water phantom. The voxel dimensions of the water phantom used for the simulation was 1.0 mm^3. A line dose profile was obtained from the PSF matrix encompassing the central voxel that encloses the pencil beam. Figure 3(a) shows a reduction of the peak surface scatter dose per incident photon up to 59% when x-ray beam energy is increased from 30 keV to 70 keV. Then the peak surface scatter dose per incident photon increased up to 44% when x-ray beam energy is increased from 70 keV to 120 keV. Figure 3(b) shows a reduction of the peak scatter to primary dose ratio of 48% when the x-ray beam energy is increased from 40 keV to 120 keV.

Figure 4 shows the backscatter factors on the center of the field as a function of keV for different field size (5 cm, 10 cm and 20 cm). For all field sizes, the backscatter factor increases first with energy and reaches a maximum between 40 keV and 60 keV, after which it decreases.

Figure 5 shows that surface scatter dose is reduced when a bone was underneath the soft tissue layer compared to a homogeneous water phantom, and the reduction increases for thicker bone layers. Because of bone's higher effective atomic number and greater density, it has larger photoelectric cross-section than water. Therefore, the bone layer absorbing the low energy photons and attenuating both primary and backscattered photons results in reduced backscatter. This reduction is increased for thicker bone layers due to its increased attenuation of both primary and backscattered photons.

Figure 6 and Figure 7 show that the surface dose reduction due to bone is less with increasing water thickness on the entrance surface above the bone layers. This is because the water produces more backscatter than the bone and the reduction of backscatter by bone layers is reduced by the water. When the water thickness above the bone layer was 20 mm, the BSF determined by convolution of the PSF was 1.39, which is close to the BSF of 1.37 calculated by EGSnrc for the full field.

Figure 8 shows the that the backscatter PSF becomes more forward directed and the peak increases as the angle of the incident beam relative to the surface decreases from 90° (perpendicular) to 30°. The BSF convolved from the PSF at the center of a 20×20 cm field is

1.41 at 90°, 1.45 at 60° and 1.71 at 30°, showing about a 21% increase of backscatter from 90° to 30°.

The difference of the peak of the backscatter PSF for different locations on the SK-150 phantom was up to 15% as shown in Figure 9 due to differences in the bone/soft tissue thicknesses. However, after convolution of the PSF over an area of 20×20 cm^2, the BSF for the lateral head location is 1.34 which is only slightly smaller than the BSF for the back of the head location which is 1.38.

4. CONCLUSIONS

In this work, we investigated the backscatter PSF for different x-ray beam energies, different soft tissue thickness on the entrance surface above the underlying bone, different bone thickness under the soft tissue and different entrance beam angles on phantoms. The results show a reduction of the peak scatter to primary dose ratio of 48% when the x-ray beam energy is increased from 40 keV to 120 keV. The surface backscatter dose was reduced when bone was underneath the soft tissue layer compared to a homogeneous water phantom. The reduction increases for thinner soft tissue on the entrance surface above the bone and for thicker bone layers. The backscatter factor increased about 21% when the angle of the incident beam relative to the entrance surface decreased from 90° to 30°. The difference of backscatter PSF for different locations on the SK-150 phantom was up to 15%. This study expands the scope of skin dose determination for fluoroscopically-guided interventions through the use of pencil beam backscatter convolution for irregularly-shaped or modulated beams. Knowing how the backscatter PSF varies with the parameters investigated here will allow the most appropriate PSF to be used to improve the accuracy of skin dose calculation when using the DTS.

Acknowledgments

This research was supported in part by NIH Grant R01EB002873 and Toshiba Medical Systems Corp.

References

1. Balter S, et al. Fluoroscopically guided interventional procedures: a review of radiation effects on patient’s skin and hair. Radiology. 2010; 254(2):326–341. [PubMed: 20093507]
2. Petoussi-Henss N, et al. Calculation of backscatter factors for diagnostic radiology using Monte Carlo methods. Phys Med Biol. 1998; 43(8):2237–50. [PubMed: 9725601]
3. Martin CJ. Measurement of patient entrance surface dose rates for fluoroscopic X-ray units. Phys Med Biol. 1995; 40:823–834. [PubMed: 7652010]
4. Benmakhlouf H, et al. Backscatter factors and mass energy-absorption coefficient ratios for diagnostic radiology dosimetry. Phys Med Biol. 2011; 56:7179–204. [PubMed: 22024474]
5. Rudin S, Bednarek DR. Region-of-interest fluoroscopy. Med Phys. 1992; 19:1183–1189. [PubMed: 1435596]
6. Rudin, S., Bednarek, DR. Categorical course in Physics. RSNA Publications; 1995. Spatial shaping of the beam: collimation, grids, equalization filters, and region-of-interest fluoroscopy; p. 75-85.
7. Rudin S, et al. Clinical application of region-of-interest techniques to radiologic imaging. RadioGraphics. 1996; 16:895–902. [PubMed: 8835978]
8. Vijayan S, et al. A Real-Time Skin-Dose Mapping System for Region-Of-Interest (ROI) Fluoroscopy. Med Phys. 2015; 42:3717.

9. Vijayan S, et al. Incorporating corrections for the head-holder and compensation filters when calculating skin dose during fluoroscopically guided interventions. Proc SPIE 9412. 2015:94122I.
10. Bednarek DR, Barbarits J, Rana VK, Nagaraja SP, Josan M, Rudin S. Verification of the performance accuracy of a real-time skin-dose tracking system for interventional fluoroscopic procedures. Proc SPIE 7961. 2011:796127.
11. Vijayan S, et al. Automatic Skin-Dose Mapping for an Angiographic System with a Region-Of-Interest, High-Resolution Detector. Med Phys. 2014; 41(6):385–385.
12. Rana VK, et al. Dependence On Calibration Phantom and Field Area of the Conversion Factor Used to Calculate Skin Dose During Neuro-Interventional Fluoroscopic Procedures. Med Phys. 2014; 41(6):134–135.
13. Xiong Z, et al. A System for Automatically Calculating Organ and Effective Dose for Fluoroscopically-Guided Procedures. Med Phys. 2015; 42(6):3583.
14. Vijayan S, et al. Comparison of Kerma-Area- Product between the Micro-Angiographic Fluoroscope (MAF) and a Flat Panel Detector (FPD) as used in Neuro-Endovascular Procedures. Med Phys. 2015; 42(6):3253–3254.
15. Rana VK, Rudin S, Bednarek DR. A tracking system to calculate patient skin dose in real-time during neurointerventional procedures using a biplane x-ray imaging system. Med Phys. 2016; 43(9):5131. [PubMed: 27587043]
16. Vijayan S, et al. A system to track skin dose for neuro-interventional cone-beam computed tomography (CBCT). Proc SPIE 9783. 2016:97832X.
17. Vijayan S, et al. Integration of kerma-area product and cumulative air kerma determination into a skin dose tracking system for fluoroscopic imaging procedures. Proc SPIE 9783. 2016:97836G.
18. Xiong Z, et al. Automatic Calculation of Organ and Effective Dose for CBCT and Interventional Fluoroscopic Procedures. Med Phys. 2016; 43(6):3749.
19. Vijayan S, et al. Kerma Area Product Calculation for Non-Uniform X-Ray Fields Using a Skin Dose Tracking System. Med Phys. 2016; 43(6):3716–3716.
20. Xiong Z, et al. Lens of the eye dose calculation for neuro-interventional procedures and CBCT scans of the head. Proc SPIE 9783. 2016:97832V.
21. Vijayan S, et al. A Backscatter Point Spread Function for Entrance Skin Dose Determination. Med Phys. 2016; 43(6):3748–3749.
22. Vijayan S, et al. Skin dose mapping for non-uniform x-ray fields using a backscatter point spread function. Proc SPIE 10132–29. 2017

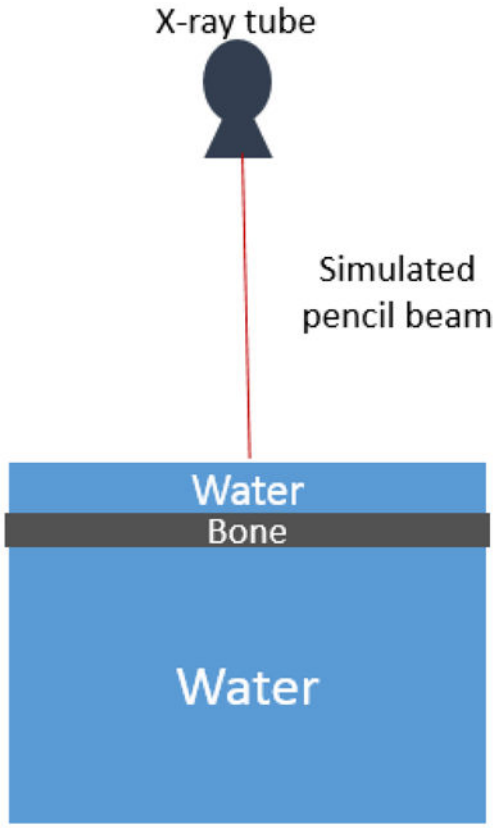

Fig. 1.
Structure of an inhomogeneous phantom containing a layer of water above a bone layer, used to determine the effect of underlying bone on the backscatter PSF.

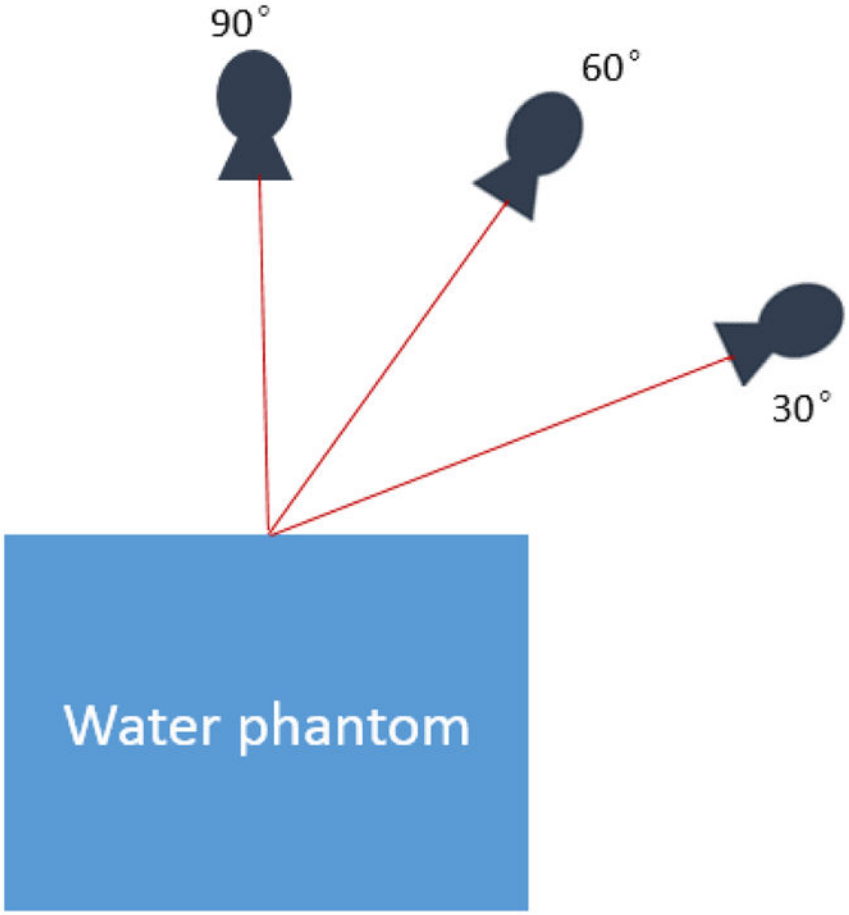

Fig. 2.
Exposure geometry for irradiation of a homogeneous water phantom by a pencil beam which was incident at different angles.

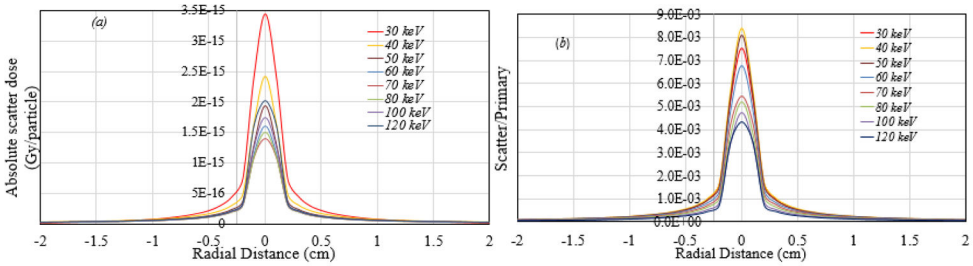

Fig. 3.

Backscatter PSF for different keVs (a) Backscatter dose per incident photon, (b) Scatter to primary dose ratio.

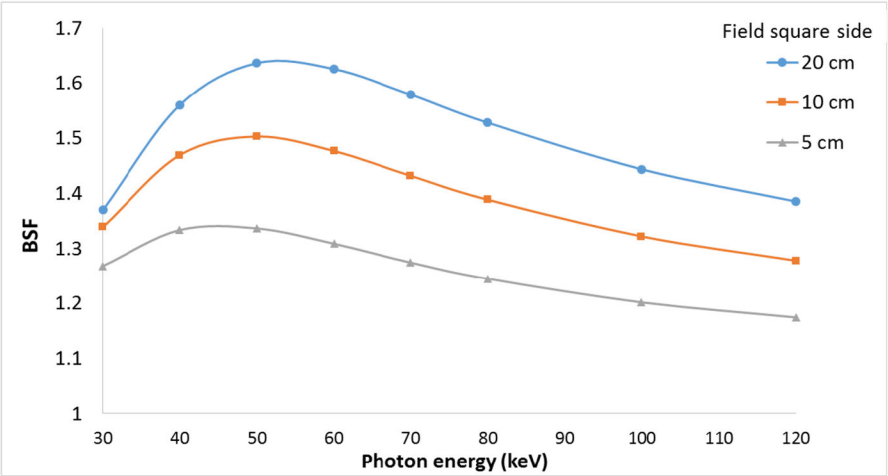

Fig. 4.

Backscatter factors at the entrance surface of a 20 cm thick water phantom for mono-energetic photons calculated from convolution of the PSF simulated by EGSnrc for the indicated reference square field sizes.

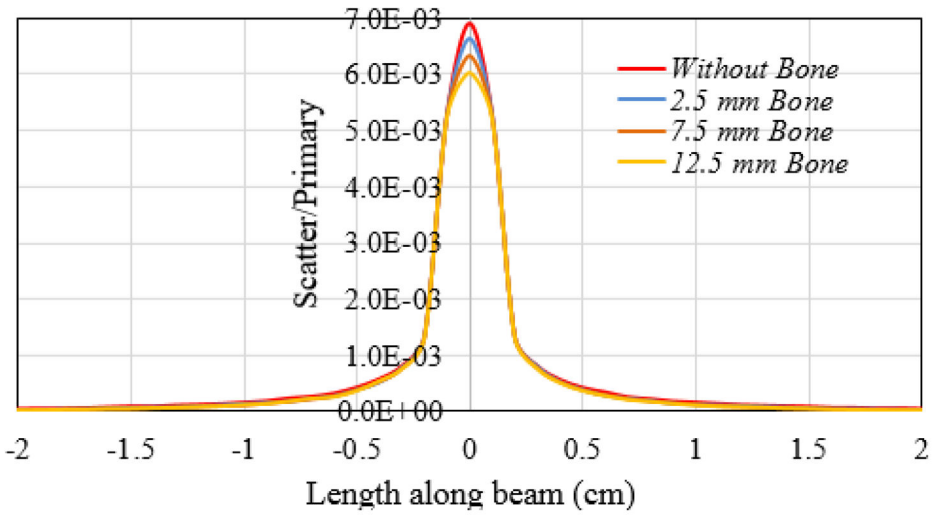

Fig. 5.

Backscatter PSF for different bone layer thickness with a constant thickness of overlying water of 5 mm.

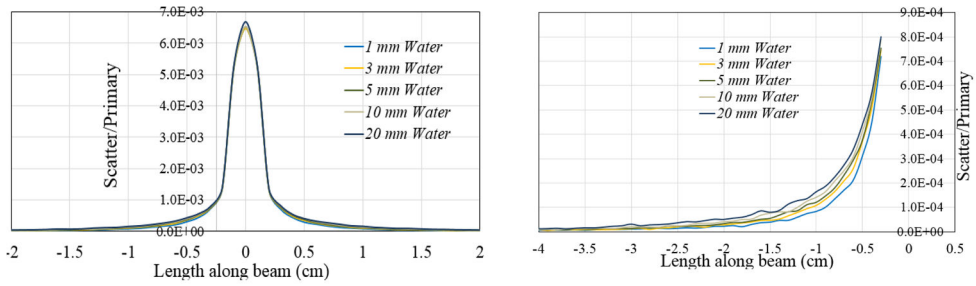

Fig. 6.

Backscatter PSF for different water thickness on the entrance surface above the bone layer. The right side figure shows an enlarged view of the PSF from −4 cm to −0.3 cm to make the differences between these PSFs more visible.

Fig. 7.

Backscatter factors as a function of water thickness on the entrance surface above the bone layer calculated by convolution of the backscatter PSF for the 20 cm square field sizes.

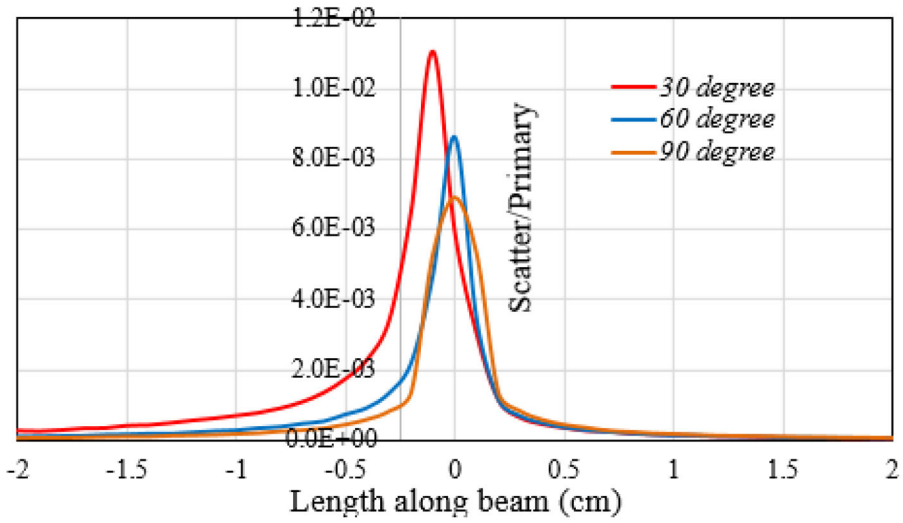

Fig. 8.

Backscatter PSF for different beam entrance angles where 90 degrees is perpendicular to the surface.

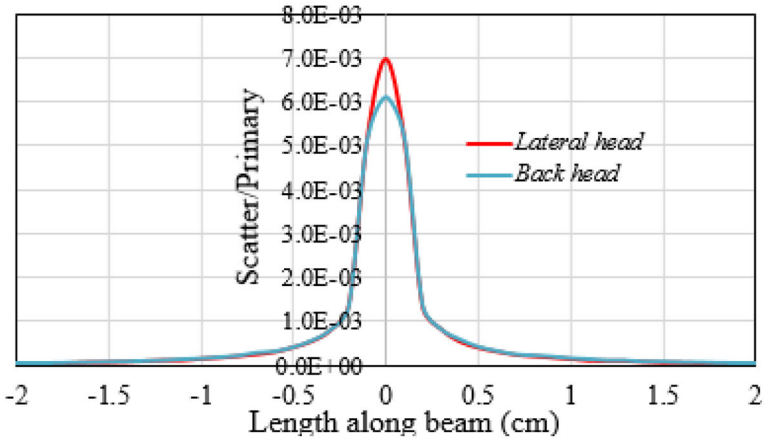

Fig. 9.
Backscatter PSF for different locations on the SK-150 head phantom.